The Use of SSM/I Data in Operational Marine Analysis*

WILLIAM H. GEMMILL AND VLADIMIR M. KRASNOPOLSKY[+]

Environmental Modeling Center, National Centers for Environmental Prediction/NWS/NOAA, Washington, D.C.

10 August 1998 and 30 March 1999

ABSTRACT

The application of Special Sensor Microwave/Imager (SSM/I) multiparameter satellite retrievals in operational weather analysis and forecasting is addressed. More accurate multiparameter satellite retrievals are now available from an SSM/I neural network algorithm. It also provides greater areal coverage than some of the initial algorithms. These retrievals (ocean surface wind speed, columnar water vapor, and columnar liquid water), when observed together, provide a meteorologically consistent description of synoptic weather patterns over the oceans. Three SSM/I sensors are currently in orbit, which provide sufficient amounts of data to be used in a real-time operational environment. Several examples are presented to illustrate that important synoptic meteorological features such as fronts, storms, and convective areas can be identified and observed in the SSM/I fields retrieved by the new algorithm. The most recent version of the neural network algorithm retrieves simultaneously four geophysical parameters: ocean-surface wind speed, columnar water vapor, columnar liquid water, and sea surface temperature, allowing the knowledge of each variable to contribute directly to better accuracy in ocean surface wind speed retrievals. The neural network wind speed data were recently incorporated as a part of operational Global Data Assimilation System at the National Centers for Environmental Prediction.

1. Introduction

Beginning in 1987, a series of Special Sensor Microwave/Imager (SSM/I) instruments was launched as a part of the Defense Meteorological Satellite Program (DMSP) (Hollinger et al. 1987). DMSP SSM/I satellites are polar-orbiting satellites with a 102-min orbit. Each satellite provides coverage over a particular ocean basin twice a day, once during a descending orbit and once during an ascending orbit. The SSM/I generates brightness temperatures in seven channels at four frequencies (19, 22, 37, and 85 GHz), each with vertical and horizontal polarization (the 22-GHz channel senses only vertical polarization). The spatial resolution is about 50 km at 19 and 22 GHz, about 30 km at 37 GHz, and 15 km at 85 GHz. The SSM/I infers brightness temperatures (BTs) from the ocean surface passively, receiving microwave radiation emitted by the ocean surface and passed through the atmosphere. The emission is effected by the surface wind speed (which changes the roughness

of the ocean surface) and by the sea surface temperature (SST). The propagation of the microwave radiation through the atmosphere is influenced by the integrated amounts of water vapor and liquid water in the atmospheric column (Wentz 1992, 1997). As a result the brightness temperatures carry signals from all these geophysical parameters and can then be converted into geophysical parameters (surface wind speed, columnar water vapor, columnar liquid water, and SST) using retrieval algorithms.

DMSP satellites have substantially increased the amount of real-time meteorological data that is acquired over the oceans, which are used subjectively (manually) by marine meteorologists to improve ocean surface weather map analyses, and objectively by numerical analysis systems to provide initial conditions for numerical weather prediction models. With three satellites in orbit (*F11, F13,* and *F14*) and with a swath width of about 1400 km for each of the satellites, high-resolution coverage is now available almost globally on a daily basis.

Empirical retrieval algorithms (or transfer functions) have been developed separately for various geophysical parameters such as surface wind speed [Goodberlet et al. (1989); Petty (1993); see also the appendix], columnar water vapor (Alishouse et al. 1990), and columnar liquid water (Weng and Grody 1994). The empirical retrieval algorithm is usually derived from a high-quality dataset that collocates the satellite brightness temperatures with buoy- and/or radiosonde-measured geo-

---

Corresponding author address: Mr. William H. Gemmill, Ocean Modeling Branch, NOAA/NWS/NCEP/EMC, 5200 Auth Road, Rm. 207, Camp Springs, MD 20746.
E-mail: wd21wg@sun1.wwb.noaa.gov

physical variables in time and space. The physically based algorithms use a large amount of such empirical data for parametrizations (Wentz 1997). The collocated matchup dataset requires a large data sample in order to represent a wide range of global meteorological events. High–wind speed events have been fairly rare in most matchup datasets because winds speeds of gale force (>17 m s^{-1}) or greater at a given time cover no more than 5% of the global ocean surface.

Some of the initially developed retrieval algorithms are based on a simple statistical technique such as linear regression and, as a result, have limited retrieval capabilities. Careful validations and evaluations of the retrievals over a period of time are required to sample a wide range of meteorological conditions and to determine the conditions for which the transfer functions do not perform well. Such validations invariably show that the initial algorithms have serious limitations in providing good-quality data over regions where weather conditions are rapidly changing. Hence the necessity to examine the possibility of making improvements to the retrieval algorithm arises (Gemmill et al. 1996).

The purpose of this paper is to address the application of improved SSM/I multiparameter satellite retrievals for use in operational marine weather analysis and forecasting. These retrievals are now available at the National Centers for Environmental Prediction (NCEP) (McPherson 1994) as a result of applying the latest SSM/I neural network algorithm to BTs from three SSM/I sensors. This algorithm provides detailed and accurate fields of meteorological variables[1] over the oceans and the coverage is extensive because of the number of satellites that are currently in operation. The new neural network algorithm derives surface wind speed (*W*), columnar water vapor (*V*), columnar liquid water (*L*), and sea surface temperature (SST) simultaneously from SSM/I brightness temperatures. Although these parameters have already been retrieved separately by other techniques, it is the simultaneous retrieval by the neural network (NN; see the appendix for brief tutorial) that is unique, allowing the information from one parameter to contribute to a better estimate of the other parameters. The parameters retrieved by the NN, when observed together, can provide information about synoptic weather patterns over the oceans (Gemmill and Krasnopolsky 1998) that is more comprehensive and internally consistent than that from a single parameter (see section 2 for details).

In order to show that the fields (*W, V,* and *L*) retrieved from SSM/I can provide information about significant synoptic meteorological features like fronts, convective areas, and areas with high probability of precipitation, in section 3 we present two case studies. There three SSM/I fields are compared with 1) surface observations

(buoys and ships), 2) independent satellite winds from the second European Remote Sensing satellite (*ERS-2*) scatterometer, 3) objective (performed by computer) analysis, and 4) subjective (performed by a meteorologist–analyst) analysis provided by Marine Prediction Center. The Marine Prediction Center (MPC) of NCEP is responsible for issuance of warnings, forecasts, and guidance in text and graphical form for marine users at sea (McPherson 1994). The two major areas of responsibility of the MPC are the North Pacific and North Atlantic Oceans. This information is routinely disseminated via U.S. Coast Guard radio and the Internet. The analyses and forecasts, out to 120 h, include sea level pressure (to locate storm centers and fronts), as well as wind, significant wave height, and wave train direction. The analyses and forecasts are subjectively produced by marine meteorologists integrating information using numerical model guidance from NCEP and other operational centers, in situ surface marine weather information, satellite-derived ocean-surface observations, and various atmospheric satellite imagery. The MPC, also as part of its duties, quality-controls marine observations from ships, buoys, and automated marine coastal stations.

2. Work on improvement of accuracy of SSM/I retrievals

A retrieval algorithm relates a vector of geophysical parameters, **g**, which in our case is **g** = {*W, V, L*, SST}, to the vector of satellite measurements, **T**, which in our case is a vector of SSM/I brightness temperatures. This relationship can be symbolically represented as

$$\mathbf{g} = \mathbf{f(T)}, \qquad (1)$$

where **f** is usually called a transfer function. In the case of SSM/I the transfer function **f** is essentially nonlinear especially when the amount of moisture in the atmosphere is significant (Petty 1993; Stogryn et al. 1994). Each particular retrieval algorithm corresponds to a particular choice of geophysical parameters to retrieve (vector **g**), brightness temperatures to use (vector **T**), a mathematical (statistical) model for the transfer function **f**, and a development dataset.

Most previous SSM/I retrieval algorithms retrieve one variable at a time. The original global algorithm for retrieving ocean-surface wind speed from SSM/I was developed by Goodberlet et al. (1989) (GSW algorithm). This algorithm is based on linear regression and is primarily limited to low moisture conditions. Further, since there were only a few wind speed observations in the high range (>18 m s^{-1}) in the matchup dataset used to formulate the GSW algorithm, the algorithm could not be expected to perform well at retrieving high winds. In general, lower accuracy of high–wind speed retrievals is a common problem for most wind speed algorithms (Boutin and Etcheto 1996).

Because of atmospheric moisture contamination and

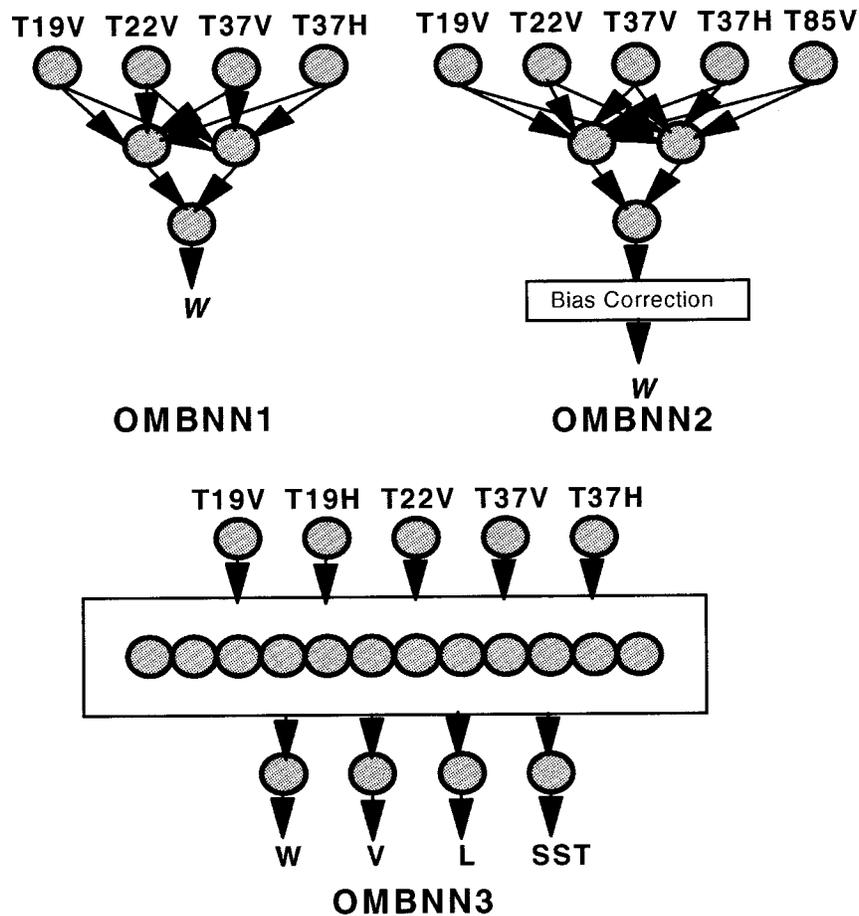[1] These fields can be seen at http://polar.wwb.noaa.gov/winds.

FIG. 1. Evolution of the SSM/I neural network architecture from OMBNN1 to OMBNN3. Brightness temperature from SSM/I channels used as input to the algorithms and geophysical parameters retrieved as outputs from the algorithms are shown. OMBNN1 has four inputs, one hidden layer with two neurons, and one output: wind speed. OMBNN2 has five inputs, one hidden layer with two neurons, and one output: wind speed. OMBNN3 has five inputs, one hidden layer with 12 neurons, and four outputs: wind speed, columnar water vapor, columnar liquid water, and sea surface temperature.

high–wind speed limitations, wind speeds cannot be accurately determined with this algorithm in areas with significant levels of atmospheric moisture (e.g., in large parts of the Tropics) and cannot be retrieved in the vicinity of storms and fronts. Petty (1993) introduced a nonlinear correction to the GSW algorithm (GSWP algorithm) that improves the accuracy of the wind speed retrievals in areas with higher amounts of the water vapor (in much of the Tropics, for example). Recently (October 1997) this version of the algorithm became operational via the shared data processing center at Fleet Numerical Meteorological and Oceanographic Center.

Several algorithms have been developed to retrieve columnar water vapor (Alishouse et al. 1990; Petty 1993) and columnar liquid water (Weng and Grody 1994; Weng et al. 1997). However, all these algorithms (including wind speed algorithms) have been developed independently using different datasets. They were formulated without taking into account the interdependen-

cy of these parameters and without accounting for the physical relationships among the parameters.

For the past five years, NCEP has concentrated on improving the accuracy of SSM/I satellite-derived ocean-surface wind speeds, columnar water vapor, and columnar liquid water for both marine meteorology applications and numerical weather prediction. A series of algorithms (see Fig. 1) has been formulated using NNs, each one more complex and accurate than the previous one. A brief review of NN theory as related to our topic is presented in the appendix. NNs were chosen because they have been highly successful in meteorological and oceanographic applications (Hsieh and Tang 1998) and in resolving complex nonlinear relationships between the sensor output and the atmospheric variable of interest (Thiria et al. 1993; Stogryn et al. 1994; Jung et al. 1998). Hence, they were able to provide an effective method for dealing with high moisture conditions while deriving wind speeds. The two first NN SSM/I wind

TABLE 1. Comparison of bias, total rms error, and high wind speed ($W > 15$ m s^{-1}) rms error, for buoy wind speed vs SSM/I wind speed, and for five SSM/I wind speed algorithms, with all errors in m s^{-1}. Errors calculated over more than 12 000 buoy–SSM/I matchups. Numbers outside the parentheses correspond to clear and in the parentheses to clear + cloudy conditions.

Algorithm	Bias	Total rmse	$W > 15$ m s^{-1} rmse
GSW[a]	−0.2 (−0.5)	1.8 (2.1)	(2.7)
GSWP[b]	−0.1 (−0.3)	1.7 (1.9)	(2.6)
Physically based[c]	0.1 (−0.1)	1.7 (2.1)	(2.6)
OMBNN3[d]	−0.1 (−0.2)	1.5 (1.7)	(2.3)

[a] Multiple linear regression (Goodberlet et al. 1989).

[b] Multiple linear regression with nonlinear water vapor correction (Petty 1993).

[c] Inversion of a physically based forward model (Wentz 1997).

[d] Neural network (Krasnopolsky et al. 1996).

speed retrieval algorithms OMBNN1 and OMBNN2 (Krasnopolsky et al. 1995a,b; 1999) were developed using the same matchup database of SSM/I brightness temperatures (from the *F8* satellite) with buoy wind speeds that was used to develop the GSW algorithm.

More recently, a rather comprehensive SSM/I and buoy matchup dataset was provided by the Naval Research Laboratory (NRL) for algorithm development. The NRL dataset contains more data and has better coverage of high wind events than the previous dataset used by GSW. Further, other high-latitude SSM/I ocean–weather ship matchup datasets were obtained from Bristol University (D. Kilham 1996, personal communication). The NN was retrained with the new wind speed

data for one parameter (wind speed only) retrievals, but large errors at high wind speeds still occurred.

Hence, a new NN architecture was formulated (Fig. 1) that takes into account the interdependence of physically related atmospheric and oceanic parameters (wind speed, columnar water vapor, columnar liquid water, and sea surface temperature). The new OMBNN3 algorithm (Krasnopolsky et al. 1999, 1998, 1997, 1996) utilizes five SSM/I brightness temperature channels. It simultaneously produces all four parameters. This algorithm was trained to preserve proper physical relationships among these parameters. The algorithm has extended the range of wind speeds over which useful retrievals can be obtained. It not only improves the accuracy of the wind speed retrievals, especially at high wind speeds (without bias correction), but makes available three additional fields. The OMBNN3 algorithm is represented by expression [Eq. (A.3) in the appendix] where $n = 5$ (inputs T19V, T19H, T22V, T37V, T37H), $m = 4$ (outputs *W, V, L,* SST), and $k = 12$ (hidden nodes).

Table 1 indicates the importance of the inclusion of water vapor, liquid water, and SST in retrieval algorithms on the accuracy of wind speed. The GSW is the original linear algorithm, and the GSWP algorithm contains the water vapor correction suggested by Petty (1993). The rms error statistics of the OMBNN3 algorithm, which takes into account also the liquid water and SST influences, are lower than those of the GSWP algorithm over all wind speeds, and especially at wind speeds >15 m s^{-1}. Figure 2 shows the wind speed difference (buoy minus satellite wind speeds) character-
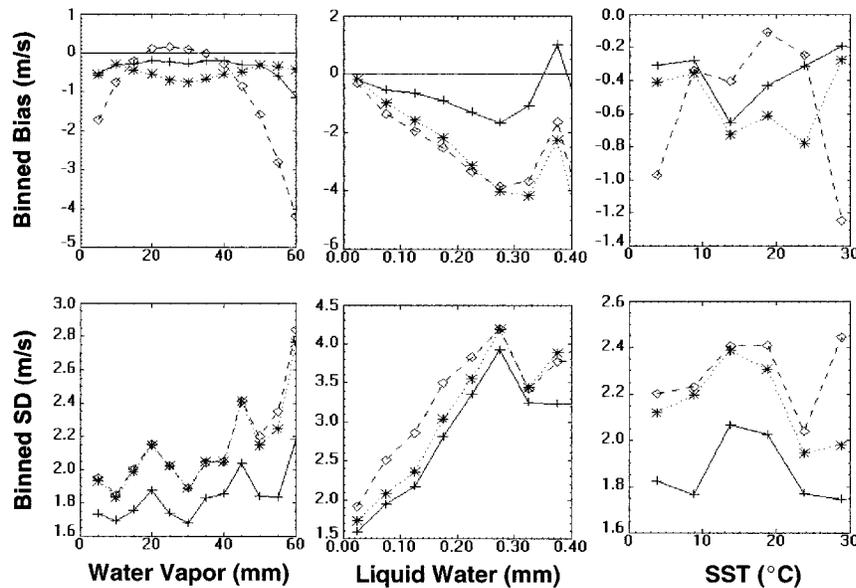

FIG. 2. Binned mean value (bias) and standard deviation (SD) of the difference between the buoy and SSM/I wind speeds vs columnar water vapor, columnar liquid water, and SST. GSW algorithm, dashed line with diamonds; GSWP algorithm, dotted line with stars; OMBNN3, solid line with crosses.

istics (retrieval errors in wind speed) as functions of three other parameters: columnar water vapor, columnar liquid water, and sea surface temperature for three algorithms GSW, GSWP, and OMBNN3. Including a nonlinear water vapor correction in GSWP reduced the bias and its dependence on the water vapor concentration (and partly on SST, which is closely related to water vapor); however, it did not reduce its dependence on the liquid water concentration. This correction also did not significantly improve the standard deviation of the differences. The OMBNN3 algorithm, with its simultaneous multiparameter retrievals, reduced the bias and its dependence on all three other parameters together with a significant improvement in the standard deviation of the differences.

The NN retrievals for columnar water vapor and columnar liquid water are in good agreement with existing SSM/I algorithms. No attempt was made to verify these retrievals against observed data because of the lack of collocated observations. The details of the development of OMBNN3 and its validation have been documented by Krasnopolsky et al. (1999, 1998, 1997, 1996). The accuracy of the SST retrievals is lower than the accuracy of Advanced Very High Resolution Radiometer SST; however, the SSTs give secondary information that improves the accuracy of the wind speed retrievals, especially at high wind speeds. Because this algorithm is inherently nonlinear, it increases areal coverage in areas with significant levels of atmospheric moisture and under more active and critical weather systems such as storms and fronts.

OMBNN3 has been extensively evaluated at NCEP using real-time data from *F10, F11, F13,* and *F14* SSM/I instruments. Simultaneous retrievals of wind speed, columnar water vapor, and columnar liquid water fields using OMBNN3 were examined to reveal significant information concerning weather patterns over the ocean. In the Global Data Assimilation System (GDAS) at NCEP, impact studies similar to those performed earlier for OMBNN2 (Yu et al. 1997) have been performed using the OMBNN3 algorithm and further positive impact was observed as compared to both GSW and OMBNN2 (T.-W. Yu 1998, personal communication). Based on these results the OMBNN3 ocean-surface wind speed retrievals were incorporated into the operational GDAS at NCEP in April 1998.

3. Interpretation of SSM/I neural network–derived data for weather analysis

In this section, we show that the three meteorological variables (ocean-surface wind speed, columnar water vapor, and columnar liquid water) that are produced simultaneously by the new OMBNN3 algorithm can provide a clear descriptive analysis of the weather over the ocean. Moreover, we show how the interpretation of the three variables together can give a more complete description of marine weather than by using the ocean wind speed data alone.

The ocean-surface wind speed data have the most direct use in marine weather analysis and weather forecasting. Although these data provide wind speed only, the extensive coverage of the three satellites depicts high-resolution wind speed patterns across synoptic weather systems. These data can be used directly to improve ocean-surface wind analyses and indirectly to improve sea level pressure analyses.

The columnar water vapor and columnar liquid water values are vertically integrated through the entire atmosphere. The columnar water vapor is also known as *total precipitable water,* which is the depth of water that would fall on the ocean if all the water vapor were condensed and precipitated. Columnar water vapor is an airmass characteristic closely related to synoptic-scale features. The primary source of water vapor is located over the warm tropical ocean. Water vapor is carried vertically by deep convection along convergent zones in the Tropics and is advected to higher latitudes by storms and low- and midlevel jet streams. As a result, regions with large gradients of columnar water vapor have been shown to be good objective indicators of the position of an ocean surface front (Katsaros et al. 1989).

The liquid water resides in clouds and is more directly related to regions of precipitation and to active weather systems such as storms and fronts (McMurdie and Katsaros 1996). Large liquid water amounts are generally associated with strong convective activity (cumulus clouds) and unstable surface weather conditions, whereas small amounts of liquid water are associated with near neutral or stable regions (stratiform clouds).

Some examples

Here we present two examples to show the use of the SSM/I data retrieved from the OMBNN3 algorithm. The examples cover two regions: one for the eastern North Pacific, and one for the western North Atlantic Ocean. For each case, a marine weather map analysis is first presented to identify major weather features over the region (Figs. 3 and 5). Marine weather maps for the North Pacific Ocean and the North Atlantic Ocean are manually produced every 6 h by the Marine Prediction Center. These analyses are based on the interpretation and intercomparison of various data sources, including the 6-h sea level pressure forecast from the global numerical weather prediction model, as a first guess, cloud imagery from Geostationary Operational Environmental Satellite and Advanced Very High Resolution Radiometer satellite systems, and quality-controlled surface data from ships, fixed and drifting buoys, and coastal stations. The analyses portray contours of sea level pressure to locate storm centers, fronts, and other important weather features and
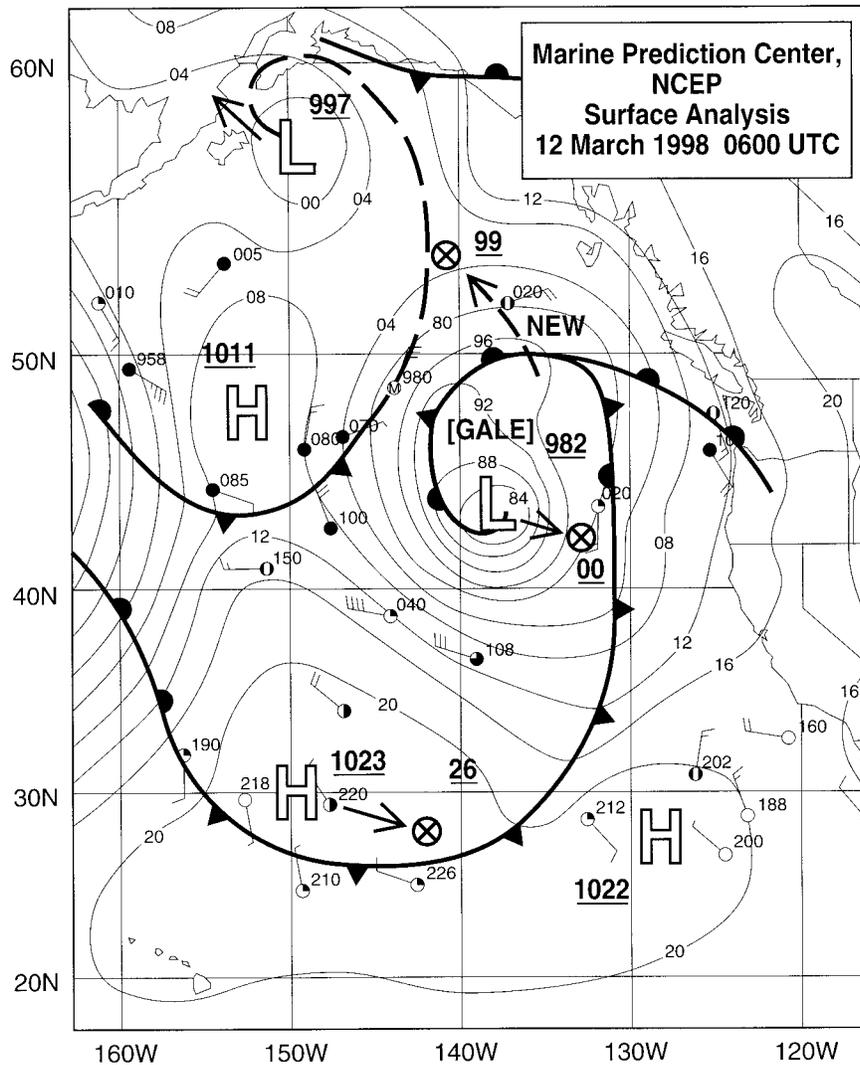
FIG. 3. Surface marine weather map for eastern North Pacific Ocean, 0600 UTC 12 Mar 1998.

to identify areas of high wind speeds, such as gale- and storm-force winds.

Each example includes a series of plots (Figs. 4 and 6): (a) SSM/I ocean-surface wind speed, (b) SSM/I columnar water vapor, (c) SSM/I columnar liquid water, (d) ocean-surface wind data from buoys and ship, (e) *ERS-2* scatterometer vector wind data that have been reprocessed at NCEP from the real-time ERS back-scatter and geometrical data records in order to improve the wind direction selection (Gemmill et al. 1996), and (f) the sea level pressure analysis available from the NCEP's GDAS. GDAS is based on objective (mathematical and statistical) methods. It updates the 3D first guess model fields using all available current datasets (i.e., satellite vertical soundings, satellite surface observations, radiosonde and aircraft data, surface data). The first-guess fields and various observational datasets are given weights (the higher the accuracy of the data, the higher their weight in analysis) to produce the "best" approximation (optimal analysis) of the current state of the atmosphere.

The plots of satellite data are within a ±3-h time window about the analysis time. The SSM/I data are a composite from three DMSP satellites (*F11, F13,* and *F14*), which together provide almost complete and extensive regional coverage.

The two cases, shown as examples here, demonstrate that SSM/I wind speeds are consistent with other data: ship, buoy, and *ERS-2* scatterometer winds; the numerical sea level pressure analysis; and the manual marine weather analysis. They also show that the SSM/I columnar water vapor and liquid water provide additional information to describe important weather features. Comparison of various plots show that each SSM/I da-
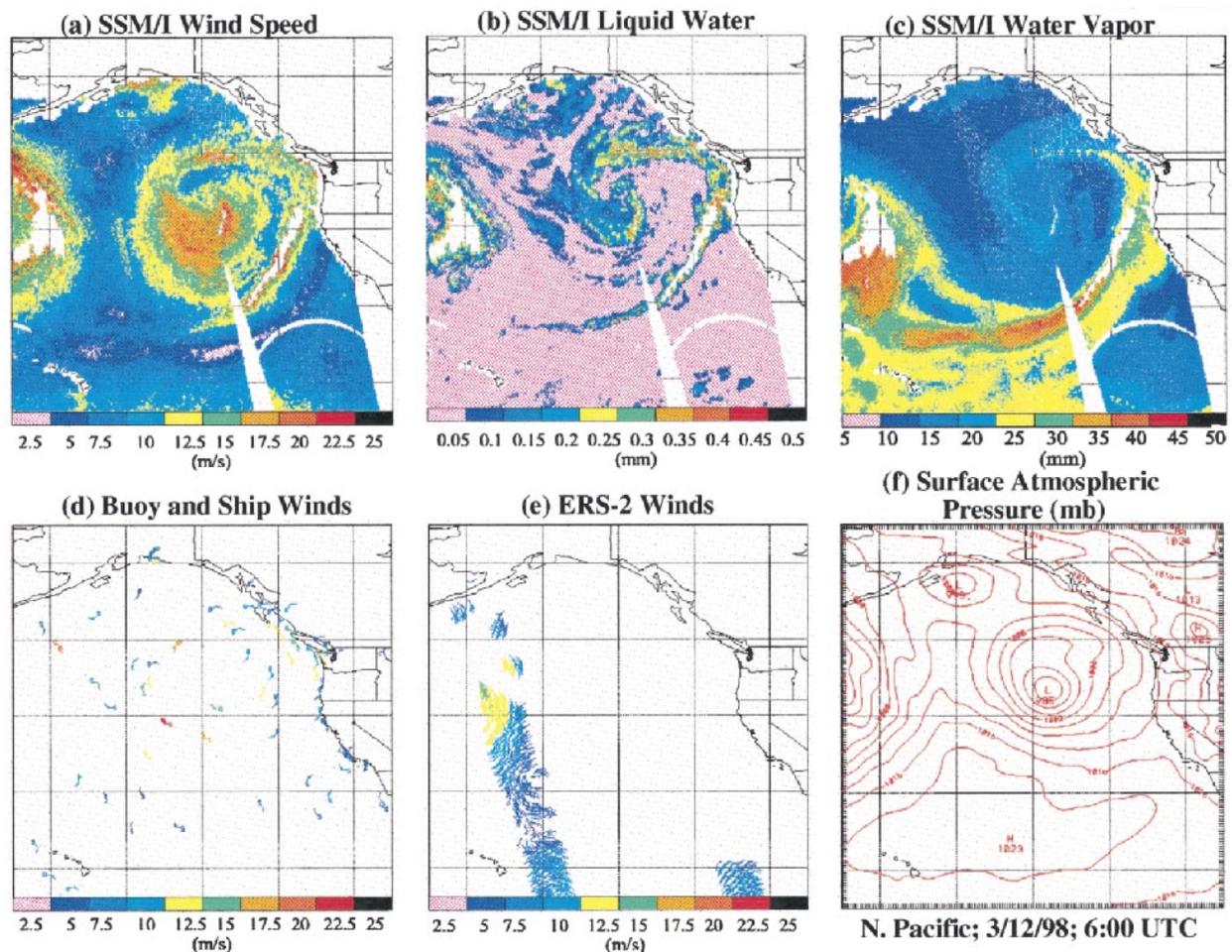
FIG. 4. (a) SSM/I-derived ocean surface wind speed data, (b) SSM/I-derived columnar liquid water data, (c) SSM/I columnar water vapor data, (d) buoy and ship wind data, (e) *ERS-2* scatterometer wind vector data, and (f) sea level pressure analysis from global analysis system over eastern North Pacific Ocean, 0600 UTC 12 Mar 1998. Each panel covers an area from 15° to 65°N and from 165° to 115°W.

taset retrieved from the SSM/I through the NN algorithm provides information that either supports or complements a consistent weather analysis interpretation.

1) EXAMPLE 1: EASTERN NORTH PACIFIC OCEAN, 0600 UTC 12 MARCH 1998

The marine weather analysis for the northeastern Pacific at 0600 UTC 12 March 1998 is presented in Fig. 3. The main weather feature in the northeast Pacific is a moderate storm with a central pressure of 982 mb, located near 43°N and 138°W, 600 n mi west of the Oregon coast. The storm itself is labeled "GALE," indicating winds above 16–17 m s^{-1}. Within its circulation, this storm has wrapped around the occlusion from the north to the northwest of the center, with a cold front to the east, located about 300 n mi from the Washington to California coasts near 131°W. The front trails back toward the west and, eventually, toward the northwest to the leading edge of the next storm, which is in the

central Pacific near the date line. There is another small low analyzed just off the southern coast of Alaska. A major high pressure ridge lies across the southern part of the region along 26°–28°N. Winds are near 15 m s^{-1} to the southwest of the storm and about 20 m s^{-1} closer to the storm center.

The sea level pressure analysis from the global model at 0600 UTC shows little difference from the MPC analysis. The MPC analysis has the storm slightly deeper by 4 mb than the global model analysis (Fig. 4f).

The SSM/I wind field (Fig. 4a) shows the storm to be fairly circular and moderate in size. The yellow region shows the outer limit of the 10 m s^{-1} winds, and the orange region shows the gale force region southwest of the center and 20 m s^{-1} winds near the center. Due to high moisture content ($L > 0.4$–0.45 mm) that makes retrievals impossible, and due to an occasional bad scan line (SSM/I BTs are corrupted and rejected by a quality control), there are areas without wind speed data. The northward-moving occluded

front is associated with a band of high wind speeds (15 m s^{-1}). Just ahead of the eastward-moving cold front there is a wind band with winds up to 12.5–15 m s^{-1}, but the strongest winds are masked due to high moisture contamination (possible rain). The weak low south of Alaska has winds near 15 m s^{-1} along the coast. The storm farther west is already generating 20–23 m s^{-1} winds ahead of the occlusion.

The liquid water (Fig. 4b) shows a wraparound pattern along the cold front and then along the occlusion into the center. The greatest liquid water values quite likely are associated with rain areas that precede the occlusion and cold front. Lower values are indicated behind the fronts. The water vapor (Fig. 4c) shows the distinct pattern associated with the air masses. The large water vapor gradient zone has been recognized as a quantitative parameter for the location of oceanic fronts by Katsoras et al. (1989), it clearly depicts the location of the cold front. The water vapor shows a strong flow of moist air moving from north of Hawaii to the U.S. northwest coast.

The in situ buoy and ship wind data (Fig. 4d) are plotted four times a day at the standard synoptic times of 0000, 0600, 1200, and 1800 UTC. The satellite data are taken within 3 h of the surface ship and buoy data. Although the winds show the circulation associated with a storm, the intensity and location of the storm center cannot be determined from the ship and buoy data alone. Determination of those values is aided by the SSM/I-derived data, and where there are in situ surface wind reports, they corroborate the values of the SSM/I-derived wind speed data. Likewise, the *ERS-2* scatterometer wind data (Fig. 4e) and SSM/I wind data are in close agreement.

2) EXAMPLE 2: WESTERN NORTH ATLANTIC OCEAN, 1200 UTC 25 FEBRUARY 1998

The main weather feature in the western North Atlantic is a moderate storm with a central pressure of 984 mb, located near 42°N and 68°W, 600 n mi off the coast of New England (Fig. 5). That storm is labeled "STORM," indicating wind speeds above 24 m s^{-1}. An occlusion extends from the north to the southeast, with a cold front far out in the Atlantic trailing back to Jamaica. There is another major storm off Greenland, and a minor storm in the central Atlantic near 30°N. A major high pressure ridge is oriented north–south, centered at 48°N and 42°W (1037 mb). The plotted winds show a rather large region of strong winds (17–23 m s^{-1}) within 600–800 n mi of the center of the storm. The sea level pressure analysis from the numerical global model at 1200 UTC (Fig. 6f) shows little difference from the manual MPC analysis (Fig. 5).

The SSM/I wind field (Fig. 6a) shows the storm to be fairly circular. The yellow region shows the outer limit of the 10 m s^{-1} winds, and the orange region shows the gale-force winds around the center of the

system with speeds to 22.5 m s^{-1}. The SSM/I data indicate 25 m s^{-1} winds for the Greenland storm. SSM/I data also indicate a band of 18 m s^{-1} winds on the western side of the weak system in the central Atlantic.

The liquid water values (Fig. 6b) are greatest to the southwest of the storm center, east of Cape Hatteras and south of Cape Cod, associated with a trough line crossing the area east of the Gulf Stream.

The water vapor (Fig. 6c) clearly delineates the air masses, but does not identify much structure with the occluded system itself, where the storm has already entrained and mixed in dryer air (low water vapor values) from higher latitudes. However, the associated fronts are clearly identified, especially by the large water vapor gradient across the southwest portion of the figure. The water vapor shows a strong flow of moist air moving from the Caribbean north into the eastern portion of the storm.

The surface wind data reports (Fig. 6d) and the corresponding satellite wind data are in close agreement. Note the region near 42°N between 50° and 60°W, where the surface wind speed data approach 25 m s^{-1}. The satellite wind speeds in that region are only slightly lower, about 22.5 m s^{-1}. Also, note the ship report of 30 m s^{-1} east of Greenland. In that area the satellite data indicate wind speeds of 25 m s^{-1}. Likewise, the *ERS-2* scatterometer winds (Fig. 6e) and SSM/I winds are in close agreement. The wind speeds and pattern are similar.

4. Summary

We have illustrated the analysis of meteorological variables retrieved over the oceans from the SSM/I by the new neural network algorithm. Comparisons with the subjective (manual) and objective analyses show that independent SSM/I retrievals provide information that is, in general, in agreement with all other available data and with the first guess obtained from the numerical weather prediction model. Moreover, the fact that assimilation of the SSM/I retrievals in GDAS gives rise to a positive impact on the accuracy of numerical weather prediction model demonstrates that SSM/I retrievals provide an additional information as compared with the other data sources.

In its latest form, the multiparameter neural network algorithm (OMBNN3) has been shown to adequately provide weather information on ocean-surface wind speed data, columnar water vapor, and columnar liquid water over a wide range of values of these parameters with accuracies that are operationally useful. Also, multiparameter retrievals preserve the correct physical relationships among the retrieved parameters. Each dataset retrieved from the SSM/I through the NN algorithm provides information that either supports or complements a consistent weather analysis interpretation. The algorithm generates high wind speeds (>15 m s^{-1})
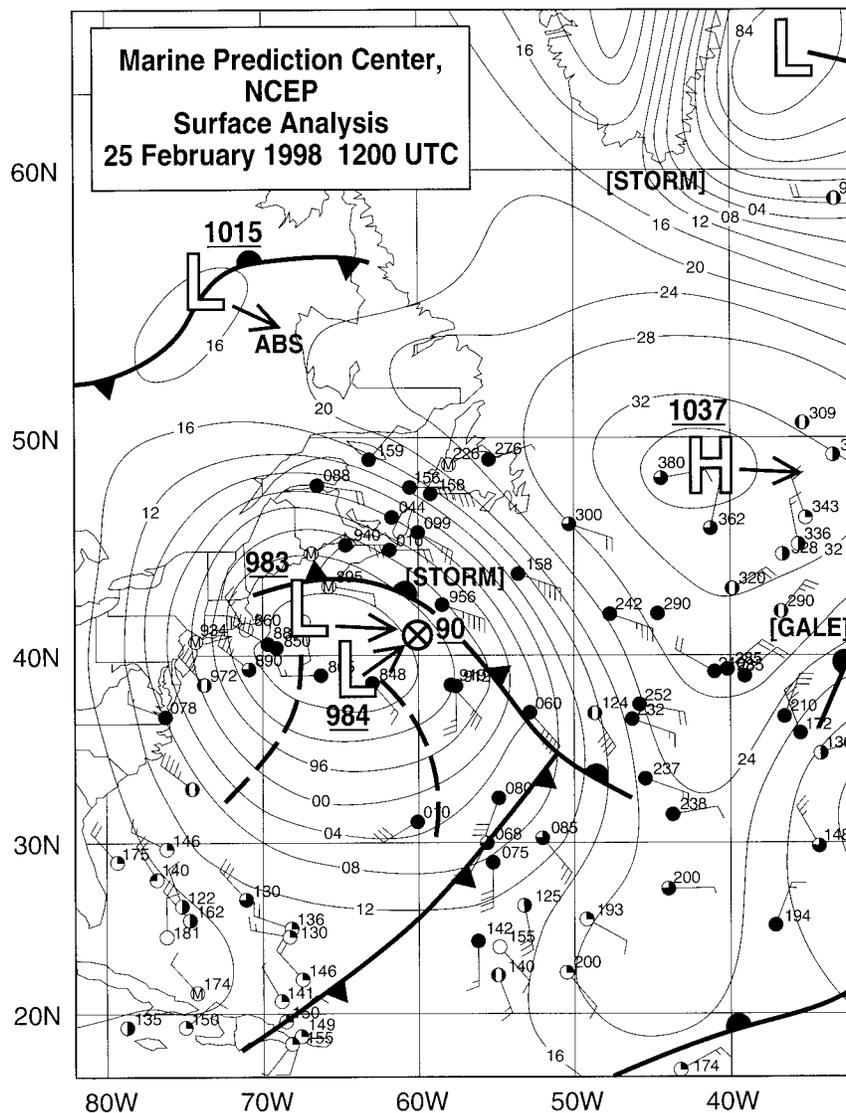
FIG. 5. Surface marine weather map for western North Atlantic Ocean, 1200 UTC 25 Feb 1998.

in areas where such winds are well supported by other data and are expected from sea level pressure analyses.

The algorithm generates columnar water vapor patterns that are able to delineate and characterize air masses; low values are associated with air masses originating in high latitudes that are cold and dry, high values are associated with air originating in tropical areas that are warm and moist, and high gradients of the columnar water vapor are related to the position of ocean surface fronts. The algorithm generates columnar liquid water patterns that are related to regions of water vapor convergence, resulting in clouds, which are closely associated with cyclones and active frontal locations.
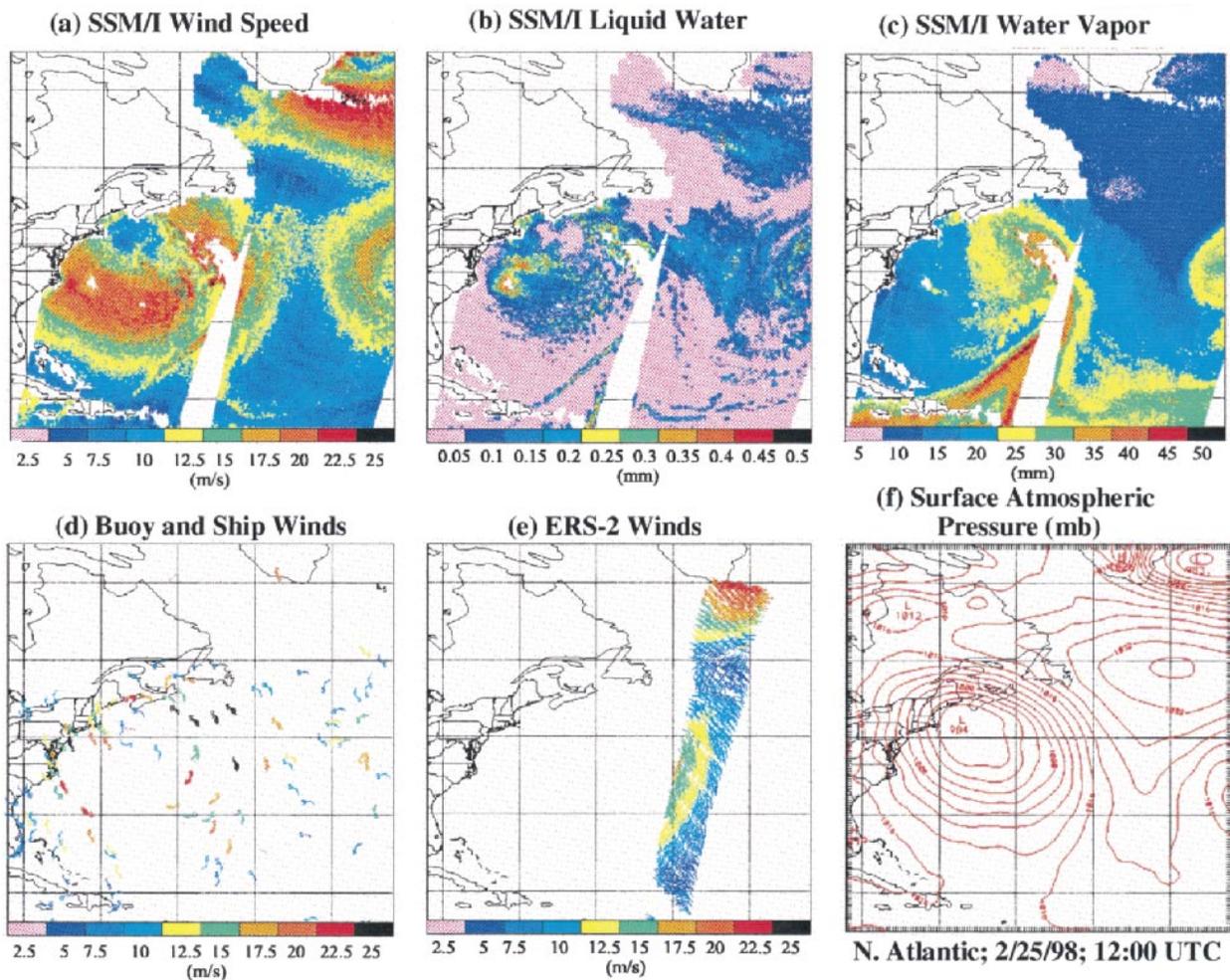
FIG. 6. (a) SSM/I-derived ocean-surface wind speed data, (b) SSM/I-derived columnar liquid water data, (c) SSM/I columnar water vapor data, (d) ship and buoy wind data, (e) *ERS-2* scatterometer wind vector data, and (f) sea level pressure analysis from global analysis system over western North Atlantic Ocean, 1200 UTC 25 Feb 1998. Each panel covers an area from 15° to 65°N and from 82° to 32°W.

APPENDIX

Neural Networks and Retrieval Algorithms

As was shown in section 2, a retrieval algorithm (transfer function) is a relationship, **f** [Eq. (1); usually nonlinear], between two vectors: a vector of geophysical parameters, **g**, and a vector of satellite measurements, **T**, **g** = **f**(**T**). Such a relationship between two vectors is called continuous mapping.

Neural networks are well suited for a very broad class of continuous approximations and mappings. Neural networks consist of layers of uniform processing elements, nodes, units, or neurons. The neurons and layers are connected according to a specific architecture or topology. Figure A1 shows a simple architecture that is sufficient for any continuous nonlinear mapping, a multilayer perceptron. The number of input neurons, *n,* in the input layer is equal to the dimension of input vector **X** (**T** in our particular case).

The number of output neurons, *m,* in the output layer is equal to the dimension of the output vector **Y** (**g** in our particular case). A multilayer perceptron always has at least one hidden layer with *k* neurons in it.

A typical neuron (processing element) usually has several inputs (components of vector **X**); one output, z_j; and consists of two parts, a linear part and a nonlinear part. The linear part forms the inner product of the input vector **X** with a weight vector $\boldsymbol{\Omega}_j$ (which is one column of the weight matrix $\boldsymbol{\Omega}$), and may also add a bias term, B_j. This linear transformation of the input vector **X** feeds into the nonlinear part of the neuron as the argument of an activation function. For the activation function, it is sufficient that it be a Tauber–Wiener (nonpolynomial, continuous, bounded) function (Chen and Chen 1995a, b). Here we use a standard activation function—the hyperbolic tangent. Then, the neuron output, z_j, can be written as
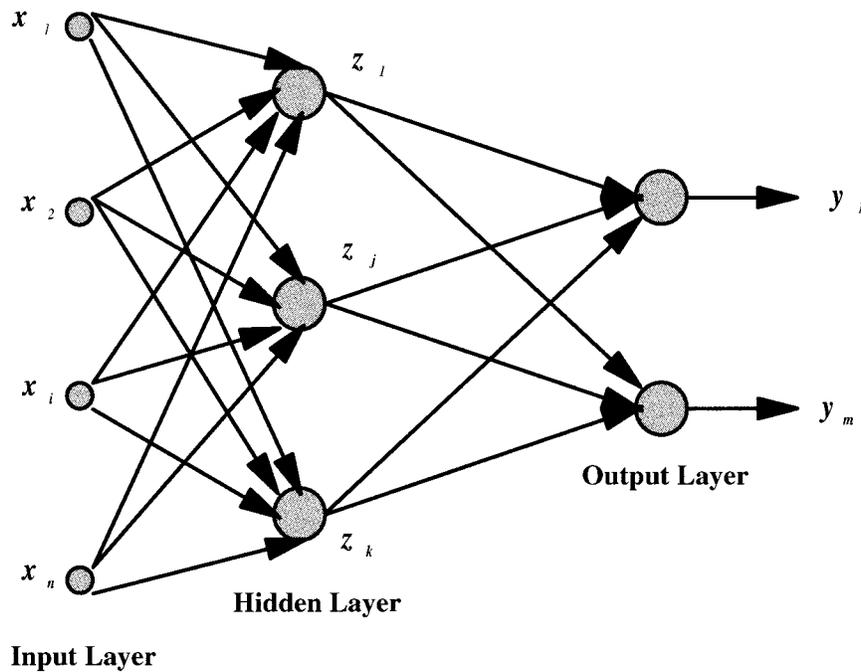
Input Layer

FIG. A1. Architecture of a simple neural network with one hidden layer.

$$z_j = \tanh\left(\sum_{i=1}^{n} \mathbf{\Omega}_{ji}^{\mathrm{T}} x_i + B_j\right)$$

$$\mathbf{\Omega} \in \mathbb{R}^{n \times k}; \qquad \mathbf{B} \in \mathbb{R}^k. \tag{A1}$$

The neuron is a nonlinear element because its output z_j is a nonlinear function of its inputs $\mathbf{X}$.

From the discussion above it is clear that the NN generally performs a continuous (and nonlinear) mapping of an input vector $\mathbf{X} \in \mathbb{R}^n$ (n is the dimension of the input vector or the number of inputs) onto an output vector $\mathbf{Y} \in \mathbb{R}^m$ (m is the dimension of the output vector or the number of outputs). Symbolically, this mapping can be written as

$$\mathbf{Y} = \mathbf{f}_{\mathrm{NN}}(\mathbf{X}), \tag{A2}$$

where $\mathbf{f}_{\mathrm{NN}}$ denotes this neural network mapping (the NN input–output relation).

For the topology shown in Fig. A1 for an NN with k neurons in one hidden layer, and using (A1) for each neuron in the hidden and output layers, (A2) can be written explicitly as

$$y_q = b_q + a_q \tanh\left\{\sum_{j=1}^{k} \omega_{qj}^{\mathrm{T}}\left[\tanh\left(\sum_{i=1}^{n} \mathbf{\Omega}_{ji}^{\mathrm{T}} x_i + B_j\right)\right] + \beta_q\right\},$$

$$q = 1, \dots, m, \tag{A3}$$

where the matrix $\mathbf{\Omega}$ and the vector $\mathbf{B}$ represent weights and biases in the neurons of the hidden layer, $\boldsymbol{\omega} \in \mathbb{R}^{k \times m}$ and the $\boldsymbol{\beta} \in \mathbb{R}^m$ represent weights and biases in the neurons of the output layer, and a_q and b_q are scaling parameters. It can be seen from (A.3) that any com-

ponent (y_q) of the NN's output vector $\mathbf{Y}$ is a complicated nonlinear function of all components of the NN's input vector $\mathbf{X}$. It has been shown (e.g., Chen and Chen 1995a, b; Funahashi 1989) that an NN with one hidden layer [e.g., NN (A3)] can approximate any continuous mapping defined on compact sets in $\mathbb{R}^n$.

For each particular problem, n and m are determined by the dimensions of the input and output vectors $\mathbf{X}$ and $\mathbf{Y}$. The number of hidden neurons, k, in each particular case should be determined taking into account the complexity of the problem. The more complicated the mapping, the more hidden neurons are required. Unfortunately, there is no universal rule that applies. Usually k is determined by experience and experiment. In general, if k is too large, the NN will reproduce noise as well as the desired signal. Conversely, if k is too small, the NN is unable to reproduce the desired signal accurately. After these topological parameters are defined, the weights and biases can be found, using a procedure that is called NN training. A number of methods have been developed for NN training (e.g., Beale and Jackson 1990; Chen 1996). Here we use a simplified version of the steepest (or gradient) descent method known as the backpropagation training algorithm.

Because the dimension of the output vector $\mathbf{Y}$ may obviously be greater than one, NNs are well suited for modeling multiparameter transfer functions (1). All components of the output vector $\mathbf{Y}$ are produced from the same input vector $\mathbf{X}$. They are related through common hidden neurons; however, each particular component of the output vector $\mathbf{Y}$ is produced by a separate output neuron that is unique.

REFERENCES

Alishouse, J. C., S. A. Snyder, J. Vongsathorn, and R. R. Ferraro, 1990: Determination of oceanic total precipitable water from the SSM/I. *IEEE Trans. Geosci. Remote Sens.,* **23,** 811–816.

Beale, R., and T. Jackson, 1990: *Neural Computing: An Introduction.* Adam Hilger, 240 pp.

Boutin, J., and J. Etcheto, 1996: Consistency of Geosat, SSM/I, and ERS-1 global surface wind speeds—Comparison with in situ data. *J. Atmos. Oceanic Technol.,* **13,** 183–197.

Chen, C. H. Ed., 1996: *Fuzzy Logic and Neural Network Handbook.* McGraw-Hill, 530 pp.

Chen, T., and H. Chen, 1995a: Approximation capacity to functions of several variables, nonlinear functionals, and operators by radial basis function neural networks. *Neural Networks,* **6,** 904–910.

——, and ——, 1995b: Universal approximation to nonlinear operators by neural networks with arbitrary activation function and its application to dynamical systems. *Neural Networks,* **6,** 911–917.

Funahashi, K., 1989: On the approximate realization of continuous mappings by neural networks. *Neural Networks,* **2,** 183–192.

Gemmill, W. H., and V. M. Krasnopolsky, 1998: Weather patterns over the ocean retrieved by neural network multi-parameter algorithm from SSM/I. *Proc. Fifth Int. Conf. on Remote Sensing for Marine and Coastal Environment,* Vol. I, San Diego, CA, ERIM Int., Inc., 395–402.

——, ——, L. Breaker, and C. Peters, 1996: Developments to improve satellite derived ocean surface wind data for use in marine analyses. Preprints, *15th Conf. Weather Analysis and Forecasting,* Norfolk, VA, Amer. Meteor. Soc., 499–500.

Goodberlet, M. A., C. T. Swift, and J. C. Wilkerson, 1989: Remote sensing of ocean surface winds with the Special Sensor Microwave/Imager. *J. Geophys. Res.,* **94,** 14 547–14 555.

Hollinger, J., R. Lo, G. Poe, R. Savage, and J. Pierce, 1987: Special Sensor Microwave/Imager user's guide. Naval Research Laboratory Tech. Report, 120 pp.

Hsieh, W. W., and B. Tang, 1998: Applying neural network models to prediction and data analysis in meteorology and oceanography. *Bull. Amer. Meteor. Soc.,* **79,** 1855–1870.

Jung, T., E. Ruprecht, and F. Wagner, 1998: Determination of cloud liquid water path over the ocean from special sensor Microwave/Imager (SSM/I) data using neural networks. *J. Appl. Meteor.,* **37,** 832–844.

Katsaros, K. B., I. Bhatti, L. A. McMurdie, and G. W. Petty, 1989: Identification of atmospheric fronts over the ocean with microwave measurements of water vapor and rain. *Wea. Forecasting,* **4,** 449–460.

Krasnopolsky, V. M., L. C. Breaker, and W. H. Gemmill, 1995a: A neural network as a nonlinear transfer function model for retrieving surface wind speeds from the Special Sensor Microwave/Imager. *J. Geophys. Res.,* **100** (C6), 11 033–11 045.

——, W. H. Gemmill, and L. C. Breaker, 1995b: Improved SSM/I wind speed retrievals at high wind speeds. NMC/OPC Tech. Note Contrib. 111, National Meteorological Center, 45 pp. [Available from National Centers for Environmental Prediction, National Weather Service, Camp Springs, MD 20746.]

——, ——, and ——, cited 1996: A new transfer function for SSM/I based on an expanded neural network architecture. NCEP Tech. Note OMB Contrib. 137, National Centers for Environmental Prediction, 38 pp. [Available online at http://polar.wwb.noaa.gov/omb/papers/tn137/tnombnn3.html.]

——, ——, and ——, 1997: Ocean surface retrievals from the SSM/I using neural networks. *Proc. Fourth Int. Conf. Remote Sensing for Marine and Coastal Environment,* Orlando, FL, ERIM Int., Inc., II-164–II-173.

——, ——, and ——, 1998: A neural network multi-parameter algorithm for SSM/I ocean retrievals: Comparisons and validations. *Proc. Fifth Int. Conf. Remote Sensing for Marine and Coastal Environment,* San Diego, CA, ERIM Int., Inc., I-36–I-43.

——, ——, and ——, 1999: A multi-parameter empirical ocean algorithm for SSM/I retrievals. *Can. J. Remote Sens.,* in press.

McMurdie, L. A., and K. B. Katsaros, 1996: Satellite derived integrated water vapor and rain intensity patterns: Indicators for rapid cyclogenesis. *Wea. Forecasting,* **11,** 230–245.

McPherson, R. D., 1994: The National Centers for Environmental Prediction: Operational climate, ocean, and weather prediction. *Bull. Amer. Meteor. Soc.,* **75,** 363–373.

Petty, G. W., 1993: A comparison of SSM/I algorithms for the estimation of surface wind. *Proc. Shared Processing Network DMSP SSM/I Algorithm Symp.,* Monterey, CA, NRL.

Stogryn, A. P., C. T. Butler, and T. J. Bartolac, 1994: Ocean surface wind retrievals from Special Sensor Microwave/Imager data with neural networks. *J. Geophys. Res.,* **99,** 981–984.

Thiria, S., C. Mejia, F. Badran, and M. Crepon, 1993: A neural network approach for modeling nonlinear transfer functions: Application for wind retrieval from spaceborn scatterometer data. *J. Geophys. Res.,* **98,** 22 827–22 841.

Weng, F., and N. G. Grody, 1994: Retrieval of cloud liquid water using the Special Sensor Microwave/Imager (SSM/I). *J. Geophys. Res.,* **99,** 25 535–25 551.

——, ——, and R. Ferraro, A. Basist, and D. Forsyth, 1997: Cloud liquid water climatology from the Special Sensor Microwave/Imager. *J. Climate,* **10,** 1086–1098.

Wentz, F. J., 1992: Measurement of oceanic wind vector using satellite microwave radiometers. *IEEE Trans. Geosci. Remote Sens.,* **30,** 960–972.

——, 1997: A well-calibrated ocean algorithm for Special Sensor Microwave/Imager. *J. Geophys. Res.,* **102,** 8703–8718.

Yu, T.-W., M. D. Iredell, and D. Keyser, 1997: Global data assimilation and forecast experiments using SSM/I wind speed data derived from a neural network algorithm. *Wea. Forecasting,* **12,** 859–865.